I_5S Miktoarm Star Block Copolymers: Packing Constraints on Morphology and Discontinuous Chevron Tilt Grain Boundaries

Lizhang Yang, Sheng Hong, and Samuel P. Gido*

Department of Polymer Science & Engineering, University of Massachusetts Amherst, Amherst, Massachusetts 01003

Gabriel Velis and Nikos Hadjichristidis*

Department of Chemistry, University of Athens, Panepistimiopolis Zografou 15771, Athens, Greece

Received April 30, 2001

ABSTRACT: A morphological study of three I_5S six-arm miktoarm star block copolymers is presented. These miktoarm stars are comprised of five arms of polyisoprene (PI) and one arm of polystyrene (PS) joined together at a single junction point. The strong segregation limit theory for the morphological behavior of miktoarm stars predicts that these materials should form spherical morphologies, but only lamellar and cylindrical morphologies were observed by TEM and SAXS. These results are similar to previously reported discrepancies between experimentally observed morphological behaviors of miktoarm stars and the predictions of the theory. Previous work has attributed the discrepancies to the neglect of the effect of the multifunctional junction points on calculated free energies. The current results suggest that, in addition to this, geometrical packing constraints prevent the formation of morphologies such as spheres and cylinders in highly asymmetric miktoarm stars in which the minor volume fraction component would need to occupy the matrix phase. Finally, unusual *broken chevron* tilt grain boundary morphologies were observed in a lamellar I_5S material. We attribute these new structures to the asymmetric energy penalties for interfacial bending which result from the molecular asymmetry of the miktoarm stars.

Introduction

Branched and grafted molecular architectures have been shown to be an additional factor (in addition to volume fraction and degree of segregation) which affects the morphological behavior of block copolymers. Guided by the predictions of a mean field theory derived by Milner[1,2] for the morphological behavior of A_nB_m-type, miktoarm star block copolymers, work has focused on molecules with an array of architectures including A_2B stars,[3−7] A_3B stars,[8] A_nB_n stars,[9−11] A_5B stars,[12] and multigraft architectures, which may be considered to be linear combinations of miktoarm stars.[13−15] These studies have borne out the predictions of the model in general but have revealed systematic discrepancies. In the current study, we further examine I_5S miktoarm star block copolymers; the molecular architecture of these materials is illustrated in Figure 1. I_5S stars have five arms of PI and one arm of PS per molecule, joined to each other at a single junction point. These materials equal the highest architectural asymmetries investigated thus far.[12]

The morphology of I_5S miktoarm stars is predicted by the Milner theory, which is strictly applicable only in the strong segregation limit. For architecturally and conformationally asymmetric block copolymer stars of type A_nB_m, the theory predicts morphology as a function of B component volume fraction, ϕ_B, and a molecular asymmetry parameter, $\epsilon = (n_A/n_B)(l_A/l_B)^{1/2}$. Here, n_A and n_B are the numbers of arms of block materials A and B, and $l_i = (V_i/R_i^2) = v_i/b_i^2$. V_i and R_i are the volume and radius of gyration of one arm of polymer i, while v_i is the segmental volume and b_i the statistical segment length of component i. Using segmental volumes of 132 Å^3 (PI) and 176 Å^3 (PS) and statistical segment lengths of 6.8 Å (PI) and 6.9 Å (PS), an ϵ of 4.4 is calculated for these materials.[16,17] The samples characterized have PS volume fractions of 0.58 (I_5S-58), 0.46 (I_5S-46), and 0.37 (I_5S-37).

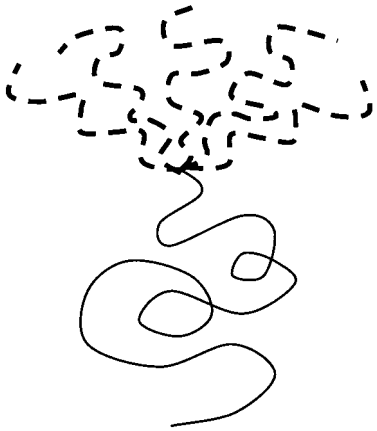

Figure 1. Illustration of the molecular architecture of an I_5S miktoarm star block copolymer.

Experimental Section

Three I_5S miktoarm stars of PI and PS were synthesized using anionic polymerization and controlled chlorosilane chemistry. The synthesis of the A_5B nonlinear block copolymers has been described in detail elsewhere.[18] All manipulations were performed in glass reactors under high vacuum. The reactors were previously washed with benzene solution of *n*-butyllithium and rinsed with benzene. Benzene was the solvent for all polymerizations and linking reactions. The PS and PI arms were synthesized separately using *sec*-butyllithium as initiator and then linked together with the hexafunctional chlorosilane 1,2-bis(trichlorosilylethane) (Si_2Cl_6). The key synthetic step was the preparation of PS−Si_2Cl_5 from PS−Li and Si_2Cl_6. The

* To whom all correspondence should be addressed.

10.1021/ma010737o CCC: $20.00
Published on Web 11/17/2001

Table 1. Molecular and Morphological Characterization Information

			I_5S-58	I_5S-46	I_5S-37
PS arm	M_n (g/mol)	MO	105 000	78 000	53 000
	M_w/M_n	SEC	1.03	1.04	1.03
PI arm	M_n (g/mol)	MO	16 300	16 300	16 300
	M_w/M_n	SEC	1.03	1.03	1.03
overall	M_n (g/mol)	MO	180 000	162 000	133 000
	M_w (g/mol)	LALLS	193 000	173 000	141 000
	M_w/M_n	SEC	1.07	1.07	1.06
	mass % PS	^{1}H NMR	61	49	40
	mass % PS	UV/SEC	60	47	37
	mass % PS	calc	58	48	40
	vol % PS		58	46	37
	$2\pi/q^*$ (±0.5 nm)		49.7	52.1	47.0
	predicted morphology		sphere	sphere	sphere
	observed morphology		lamella	cylinder	cylinder

I_5S architecture was then obtained by reaction of PI−Li with PS−Si_2Cl_5.

Table 1 lists the molecular characteristics of each sample. Membrane osmometry (MO) was performed in toluene at 35 °C. Size-exclusion chromatography (SEC) with both refractive index and UV detectors (λ = 262 nm) was performed in tetrahydrofuran at 30 °C on individual PI and PS arms prior to silane coupling as well as on the overall miktoarm architectures. Vapor pressure osmometry (VPO) was performed in toluene at 50 °C. Proton nuclear magnetic resonance (^{1}H NMR) was used to determine the weight fraction of PS in each sample. Finally, the weight fraction of PS in each sample was calculated by dividing the PS arm M_n, as measured by MO, by the total M_n of the star, $M_n(\mu) = 5(M_n(\text{PI})) + M_n(\text{PS})$. PS volume fraction was calculated for each sample using the mass fraction of PS measured by ^{1}H NMR and bulk densities.[19]

Bulk films were cast from 4 wt % solutions in toluene, a nonselective solvent for PI and PS.[20] Films approximately 2 mm thick were formed by allowing the solvent to evaporate slowly over a period of 2 weeks. The films were let stand at room temperature and atmospheric pressure for an additional week and then placed under vacuum at room temperature for 1 week to remove any residual solvent from the bulk material. The samples were subsequently annealed under vacuum for 1 week at 120 °C. At 120 °C, the calculated value of χN for the sample of lowest molecular weight (I_5S-37) is around 118, using a χ value of 0.071 for PS and PI at 120 °C.[21] Thus, the morphologies are strongly segregated. The samples were then cooled under vacuum to room temperature over a period of several hours.

Sample morphology was characterized using a combination of transmission electron microscopy (TEM) and small-angle X-ray scattering (SAXS). To prepare thin sections for microscopy, a Leica Ultracut UCT microtome equipped with a Leica EM FCS cryogenic sample chamber operated at −110 °C was used to cut sections approximately 500 Å in thickness. The sections were collected on TEM grids and stained 4 h in OsO_4 vapor. A JEOL 100CX TEM, operated at an accelerating voltage of 100 kV, was used to image the stained sections. SAXS data were collected at the Advanced Polymers Beamline (X27C), located at the National Synchrotron Light Source at Brookhaven National Laboratory (BNL), Upton, NY. Two-dimensional scattering patterns were collected on Fujitsu image plates and then read by a Fujitsu BAS 2000 image plate reader. Custom software at BNL was used to subtract background, correct for incoherent scattering, and perform circular averaging. Data were collected for a wavelength of 1.307 Å and a camera length of 1410 mm.

Results

The results of the morphological characterization for the three I_5S materials are listed in Table 1. Circularly averaged, I vs q SAXS data for all three I_5S samples are shown in Figure 2. The excellent long-range order

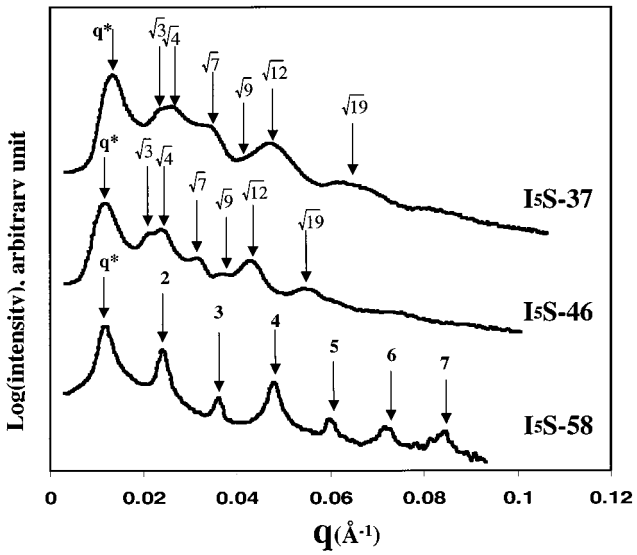

Figure 2. Plot of log(I) vs q SAXS data.

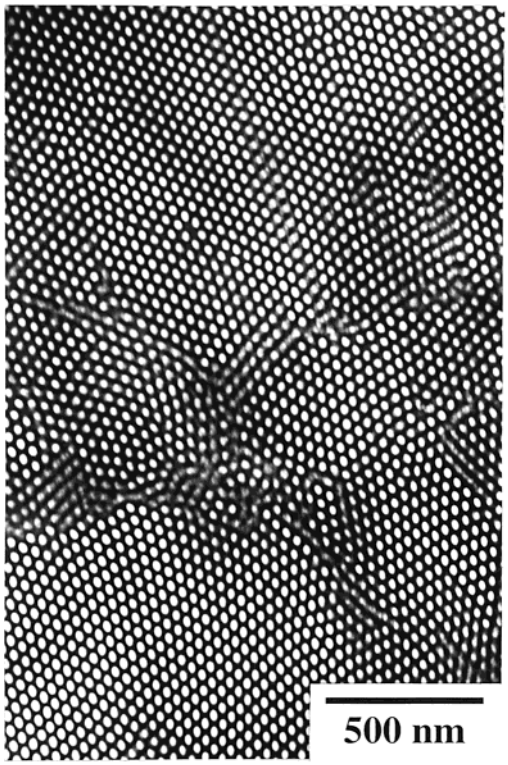

Figure 3. TEM micrographs of cylinder sample I_5S-46.

exhibited by these samples is indicated by multiple higher-order reflections. The q_n/q^* ratio of 1, $\sqrt{3}$, $\sqrt{4}$, $\sqrt{7}$, $\sqrt{9}$, $\sqrt{12}$, $\sqrt{19}$ ... indicate that I_5S-37 and I_5S-46 form hexagonal morphologies. Here, q^* is the scattering vector of the lowest angle primary scattering peak, and q_n is the series of all scattering vectors for which peaks are observed. For I_5S-58, the scattering vectors of the peaks occurring at integral multiples of q^* indicate a lamellar morphology. From the SAXS data, the lamellar long period of I_5S-58 was found to be 49.7 ± 0.5 nm. The scattering vector ratios found from the SAXS on I_5S-46 and I_5S-37 were consistent with cylinders on a hexagonal lattice with (100) spacings of 52.1 ± 0.5 and 47.0 ± 0.5 nm, respectively. Figure 3 shows a representative TEM micrograph of the cylindrical sample I_5S-46; I_5S-37 formed a similar cylindrical morphology.

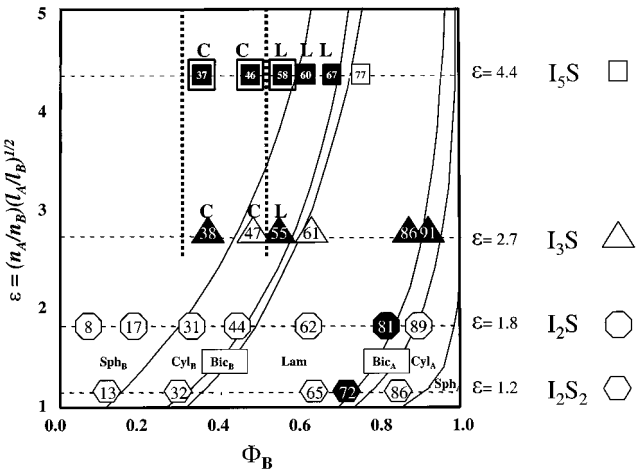

Figure 4. Morphology diagram generated by the Milner model. Morphology is given for the volume fraction of the B component, ϕ_B, and molecular asymmetry, ϵ. Shaded symbols indicate a sample whose morphology disagrees with that predicted by theory. Boldly outlined symbols indicate samples characterized in this study. The numbers in the symbols indicate the sample compositions. (For I_2S, I_3S, and I_5S, these numbers are PS volume percentages, and for the I_2S_2 samples the numbers are PI volume percentages.)

Discussion

The three I_5S samples characterized in this paper are plotted on the morphology diagram in Figure 4 along with data from samples from four previous studies involving A_2B, A_3B, A_2B_2, and A_5B miktoarm star block copolymers.[5,8,10,12] Those samples found to have morphological behavior differing from their theoretically predicted morphologies are shaded. This figure reveals an increase in the frequency of discrepancies between predicted and observed behaviors with increasing molecular asymmetry. As indicated in Figure 4, the theory predicts that the three I_5S samples of this study should form spheres. Sample I_5S-58 is found experimentally to form a lamellar morphology, and both samples I_5S-46 and I_5S-37 are found to form cylinders of PS. This discrepancy is in agreement with the general trend observed in prior studies.

As with previous studies, samples that disagree with theoretical predictions exhibit morphologies that should occur at lower ϵ for a given ϕ_B or at a higher ϕ_B for a given ϵ. For example, Beyer, Gido, and co-workers[12] found that their I_5S-60 (PS volume fraction 0.60) sample formed lamellae instead of the predicted cylinder of PS. Data from this previous study are plotted in Figure 4. While ϵ for I_5S-60 was calculated to be approximately 4.4, for the same volume fraction, lamellae occur at a maximum of $\epsilon \approx 3.0$. Alternately, for $\epsilon = 4.4$, cylinders are predicted to occur for ϕ_B greater than 0.59 but are observed at ϕ_B of 0.37. If similar comparisons are made for all the samples that disagree with the theory, one finds that the overestimation of morphological shift increases with asymmetry; slight discrepancies at low values of ϵ become greater as asymmetry increases.

Recently, Gido and co-workers[10,14] and others[22,23] have postulated that discrepancies between the Milner theory and experimental results, as illustrated in Figure 4, are a result of additional chain stretching inherent in the mikoarm star architecture due to crowding of multiple arms linked to a single junction point. Our current data suggest that, as architectural asymmetry (arm number asymmetry) becomes large, geometric packing constraints also exert an important influence on morphology. Milner's calculation was based on the assumption of a rounded Wigner−Seitz cell surrounding each domain.[1] In order for cylindrical and spherical domains to fill space, they must occupy true, space-filling polyhedral Wigner−Seitz cells and deform to fill the corners of these cells.[2,24] Therefore, the energies calculated with the rounded cell approximation (upon which Figure 4 is based) represent lower bounds. As illustrated in Figure 5b, when the volume fraction of the component which forms the core of a spherical morphology is small (as in diblock copolymers), packing problems are not very important. However, as the molecule becomes more and more asymmetric, the volume fraction of the multiarm component on the convex side of the interface may decrease to the point where it approaches the volume fraction of the interstitial space in a close packing of spheres as in Figure 5d. For example, at $\epsilon = 5$ and $\phi = 0.6$, the morphology diagram (Figure 4) predicts a spherical morphology with the 0.6 volume fraction component inside the spheres and only 0.4 volume fraction in the matrix between spheres. However, the maximum volume fraction that solid spheres in a bcc packing can occupy is only 0.65. Real spherical block copolymer domains, even with high degrees of architectural asymmetry as illustrated in Figure 5c, will not be able to achieve or even closely approach the solid contact limit for packing density of the domain cores, due to the severe conformational distortions which would be required for the corona blocks to fill the interstitial regions of the structure (corners of the Wigner−Seitz cell).[24] Thus, we expect that geometric packing limits will prevent increasing shifts to higher ϕ of the true experimentally determined order−order transition lines in Figure 4 as ϵ becomes large. A similar geometric packing limit will also apply to the cylindrical morphology. At these limits the order−order transitions will become vertical lines on the morphology diagram. In Figure 4, we have sketched the approximate positions, based on experimental data, of geometrical packing limits for spherical and cylindrical morphologies.

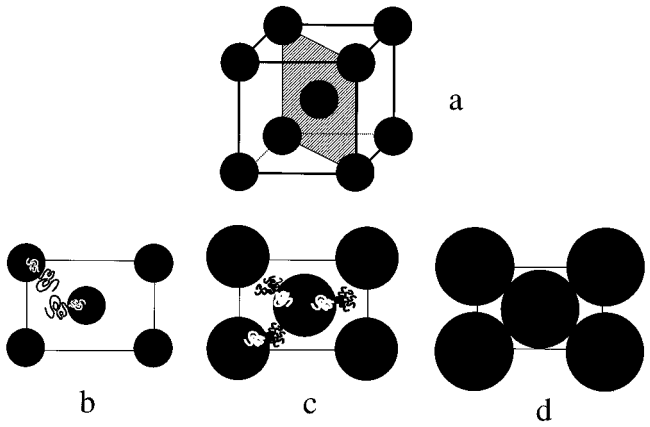

Figure 5. Geometrical packing constraints in the bcc sphere morphology: (a) the 110 plane in the bcc sphere structure; (b) illustration of chain packing in the 110 plane for diblock spheres with a large volume fraction in the matrix between spherical domains; (c) illustration of chain packing in the 110 plane for I_5S molecules in the spherical geometry with a smaller volume fraction in the matrix; (d) 110 plane of bcc spheres in the hard contact limit at 0.65 spherical volume fraction.

In the lamella forming sample, I_5S-58, unusual chevron tilt grain boundary morphologies were observed, as shown in Figure 6. Previous experimental[25−28] and

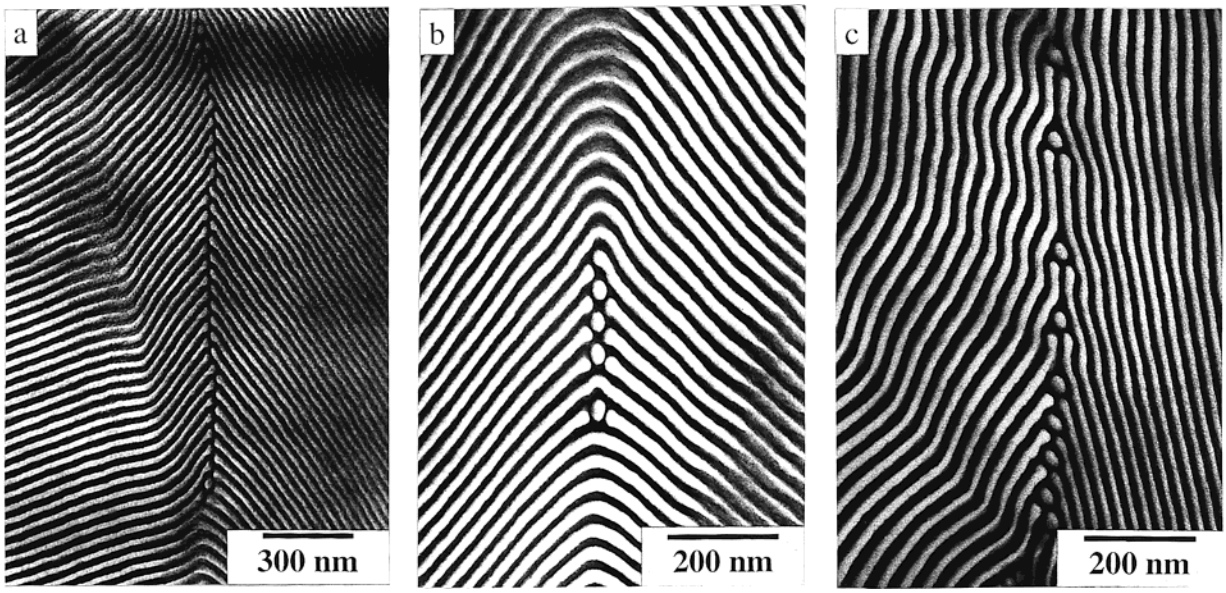

Figure 6. I_5S-58 symmetric tilt grain boundaries: (a) broken chevron, (b) broken chevron with cylinders, (c) broken Ω with cylinders.

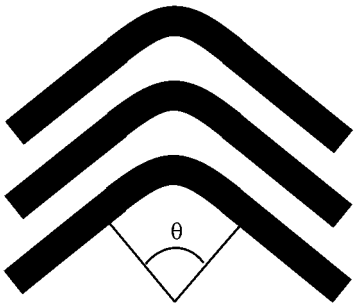

Figure 7. Schematic of commonly observed chevron tilt boundaries.

theoretical studies[29,30] of symmetric tilt grain boundaries in diblock copolymers have reported chevron tilt boundaries, as illustrated in Figure 7, in which lamellar layers retain their continuity while bending cooperatively in a narrowly defined boundary region. Figure 6 shows what we will call broken chevrons that occur in the I_5S material. In Figure 6a, the lamellae on both sides of the boundary terminate at the boundary in rows of semicylindrical end caps similar to those observed in T-junction tilt boundaries.[25,31] In Figure 6b, some lamellae terminate at the boundary in semicylindrical end caps and additionally individual complete cylinders occupy the symmetry plane of the chevron boundary. We will call this type of boundary a broken chevron with cylinders. Previous work[25,29,30] showed that at high tilt angles the lamella forming a chevron boundary develop protrusions parallel to the plane of the boundary resulting in Ω and extended-Ω variants of the chevron. The protrusions are necessary in order to fill space to constant density in the plane of the chevron grain boundary at high tilt angles. Figure 6c shows that the I_5S material forms a broken form of the Ω-boundary with additional cylindrical domains in the plane of the boundary. Recently Qiao and Winey[28] have published TEM images of Ω-boundaries in diblock copolymers formed in sheared samples that also contain some cylindrical domains localized in the plane of the boundaries. Unlike Figure 6c, the lamellae involved in Winey's chevrons remain continuous across the grain boundaries.

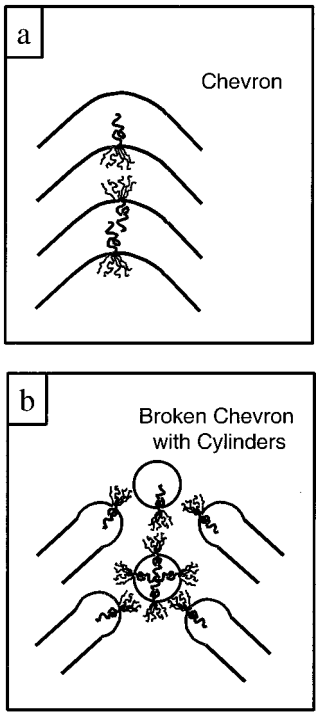

Figure 8. (a) Illustration of chevron tilt boundaries for I_5S samples. (b) Illustration of broken or discontinuous chevron tilt boundaries for I_5S samples.

We postulate that the discontinuous nature of chevron tilt grain boundaries in I_5S-58 results from an asymmetry in the energy penalties for interfacial bending due to the asymmetry inherent in the I_5S molecular architecture. At 0.58 PS volume fraction this material forms flat lamellar interfaces at equilibrium. However, bending of these interfaces is necessary to form a chevron tilt grain boundary. As shown in Figure 8a, the standard chevron boundary involves equal degrees of interfacial curvature both toward and away from the five-arm PI side of the interface. Because of crowding inherent in packing five arms of PI on the same side of the interface and the fact that curving the interface toward the PI side will exacerbate chain stretching resulting from this

crowding, it may be energetically more costly to bend the interfaces toward the PI domains than toward the PS domains in an I_5S architecture. By replacing the standard cheveron structure with a broken or discontinuous structure as illustrated in Figure 8b, it is possible to achieve the required tilt reorientation using only interfacial curvatures which put the five PI arms on the convex side of the interface. To do this, however, it is necessary to produce higher interfacial curvatures capable of generating semicylindrical end-caps on lamellae and isolated cylinders in the grain boundary plane. For this reason the broken chevron structures are only observed at relatively high tilt angles. For instance, the tilt angles of the broken chevrons in Figure 6a,b are about 90°. Presumably, as tilt angle increases, a transition occurs from continuous to discontinuous chevron structure at the point where the energy penalty for the highly unfavorable bending toward the five PI arms (Figure 8a) first exceeds the energy to form cylinders and cylindrical caps with the five PI arms on the convex side of the interfaces (Figure 8b).

Conclusions

As seen in prior studies, the Milner theory for the morphology of miktoarm star block copolymers exhibits a systematic tendency to overestimate the effect of architectural asymmetry on morphology. This tendency becomes exaggerated with increasing asymmetry as in the I_5S samples of this study. Here we report a vertical straightening of the order−order transition lines in the morphology diagram at high ϵ due to packing constraints inherent in placing a relatively small volume fraction material in the matrix around microphase-separated domains. New discontinuous chevron tilt grain boundary morphologies were observed in a lamella forming I_5S material. The discontinuity of these boundaries is thought to result from asymmetric energy penalties for bending of the lamellar interfaces. It may be more energetically costly to curve the interface toward the five arm per molecule PI side of the interface than toward the single arm per molecule PS side of the interface.

Acknowledgment. Work at the University of Massachusetts was supported by the U.S. Army Research Office, Polymer Chemistry Program, under Contract DAAD19-01-1-0544. Central Facility support from the Materials Research Science and Engineering Center (MRSEC) at the University of Massachusetts-Amherst as well as the W. M. Keck Electron Microscopy Laboratory is also acknowledged. G. V. and N. H. thank the Exxon Research and Engineering Company, NJ, and the Research Committee of the University of Athens for their financial support.

References and Notes

(1) Milner, S. T. *Macromolecules* **1994**, *27*, 2333.
(2) Olmsted, P. D.; Milner, S. T. *Macromolecules* **1998**, *31*, 4011.
(3) Hadjichristidis, N.; Iatrou, H.; Behal, S. K.; Chludzinski, J. J.; Disko, M. M.; Garner, R. T.; Liang, K. S.; Lohse, D. J.; Milner, S. T. *Macromolecules* **1993**, *26*, 5812.
(4) Matsushita, Y.; Noda, I. *Macromol. Symp.* **1996**, *106*, 251.
(5) Pochan, D. J.; Gido, S. P.; Pispas, S.; Mays, J. W.; Ryan, A. J.; Fairclough, J. P. A.; Hamley, I. W.; Terrill, N. J. *Macromolecules* **1996**, *29*, 5091.
(6) Pochan, D. J.; Gido, S. P.; Zhou, J.; Mays, J. W.; Whitmore, M.; Ryan, A. J. *J. Polym. Sci., Polym. Phys.* **1997**, *35*, 2629.
(7) Gido, S. P.; Lee, C.; Pochan, D. J.; Pispas, S.; Mays, J. W.; Hadjichristidis, N. *Macromolecules* **1996**, *29*, 7022.
(8) Tselikas, Y.; Iatrou, H.; Hadjichristidis, N.; Liang, K. S.; Mohanty, K.; Lohse, D. J. *J. Chem. Phys.* **1996**, *105*, 2456.
(9) Beyer, F. L.; Gido, S. P.; Poulos, Y.; Avgeropoulos, A.; Hadjichristidis, N. *Macromolecules* **1997**, *30*, 2373.
(10) Beyer, F. L.; Gido, S. P.; Uhrig, D.; Mays, J. W.; Tan, N. B.; Trevino, S. F. *J. Polym. Sci.* **1999**, *37*, 3392.
(11) Turner, C. M.; Sheller, N. B.; Foster, M. D.; Lee, B.; Corona-Galvin, S.; Quirk, R. P.; Annis, B.; Lin, J.-S. *Macromolecules* **1998**, *31*, 4372.
(12) Beyer, F. L.; Gido, S. P.; Veils, G.; Hadjichristidis, N.; Tan, N. B. *Macromolecules* **1999**, *32*, 6604.
(13) Lee, C.; Gido, S. P.; Poulos, Y.; Hadjichristidis, N.; Beck Tan, N.; Trevino, S. F.; Mays, J. W. *J. Chem. Phys.* **1997**, *107*, 6460.
(14) Lee, C.; Gido, S. P.; Poulos, Y.; Hadjichristidis, N.; Beck Tan, N.; Trevino, S. F.; Mays, J. W. *Polymer* **1998**, *39*, 4631.
(15) Xenidou, M.; Beyer, F. L.; Gido, S. P.; Hadjichristidis, N.; Beck Tan, N. *Macromolecules* **1998**, *31*, 7659.
(16) Gehlsen, M. D.; Bates, F. S. *Macromolecules* **1994**, *27*, 3611.
(17) Lin, C. C.; Jonnalagadda, S. V.; Kesani, P. K.; Dai, H. J.; Balsara, N. P. *Macromolecules* **1994**, *27*, 7769.
(18) Velis, G.; Hadjichristidis, N. *Macromolecules* **1999**, *32*, 534.
(19) *Polymer Handbook*; Brandrup, J., Immergut, E. H., Eds.; Wiley-Interscience: New York, 1989.
(20) Cowie, J. M. G. In *Developments in Block Copolymers − 1*; Goodman, I., Ed.; Applied Science Publishers: New York, 1982.
(21) Mori, K.; Hasagawa, H.; Hashimoto, T. *Polym. J.* **1985**, *17*, 799.
(22) Grayer, V.; Dormidontova, E. E.; Hadziioannou, G.; Tsitsilianis, C. *Macromolecules* **2000**, *33*, 6330.
(23) Matsen, M. W.; Gardiner, J. M. *J. Chem. Phys* **2000**, *113*, 1673.
(24) Gido, S. P.; Schwark, D. W.; Thomas, E. L.; Goncalves, M. *Macromolecules* **1993**, *26*, 2636.
(25) Gido, S. P.; Thomas, E. L. *Macromolecules* **1994**, *27*, 6137.
(26) Polis, D. L.; Winey, K. I. *Macromolecules* **1996**, *29*, 8180.
(27) Polis, D. L.; Winey, K. I. *Macromolecules* **1998**, *31*, 3617.
(28) Qiao, L.; Winey, K. I. *Macromolecules* **2000**, *33*, 851.
(29) Matsen, M. W. *J. Chem. Phys.* **1997**, *107*, 8110.
(30) Netz, R. R.; Andelman, D.; Schick, M. *Phys. Rev. Lett.* **1997**, *79*, 1058.
(31) Burgaz, E.; Gido, S. P. *Macromolecules* **2000**, *33*, 8739.

MA010737O